EVALUATING AGE RELATED CHANGES IN CORTICAL SUSCEPTIBILITY

By

Liam Moers Quinlan Jenkins

A capstone project submitted for Graduation with University Honors

May 6, 2026

University Honors

University of California, Riverside

APPROVED

Dr. Xiaoping Hu

Department of Bioengineering

Dr. Begoña Echeverria, Howard H Hays, Jr. Chair

University Honors

ABSTRACT

Iron deposition and demyelination are commonly observed in the aging brain and neurodegenerative diseases. Magnetic resonance imaging (MRI) allows for characterization of iron deposition and myelination in vivo. Quantitative susceptibility mapping is a MRI technique that measures magnetic susceptibility, the degree a material is magnetized in response to an applied magnetic field, and quantitative susceptibility source separation allows for the separation of paramagnetic (i.e. positive susceptibility) and diamagnetic (i.e. negative susceptibility). components. Iron is paramagnetic and myelin is diamagnetic and the magnetic susceptibility of different tissues will vary based on the relative content of iron and myelin. Here, we examine the relationship between age and susceptibility in 54 healthy older adults (aged 60-87 years; interquartile range: 65-73, median: 68, mean: 69.3 ± 6.02 years; 24 males and 30 females) recruited from the community surrounding University of California, Riverside. All subjects provided written informed consent. Statistically significant correlations were seen between age and diamagnetic susceptibility in the frontal lobe ($r = 0.412$, $p<0.01$), temporal lobe ($r = 0.286$, $p<0.01$), occipital lobe ($r = 0.402$, $p<0.01$), and parietal lobe ($r = 0.348$, $p<0.01$). No significant relationship was observed between age and the paramagnetic susceptibility component in any cortical region. The positive correlation between diamagnetic susceptibility and age may be due to grey matter volume loss. Older adults experience a loss of cortical grey matter and myelin may make up a larger percentage of brain tissue in older adults. This may lead to a relative increase in diamagnetic susceptibility.

ACKNOWLEDGEMENTS

This project would not have been possible without my faculty-mentor, Dr. Xiaoping Hu for his incredible level of support throughout the project. I would also like to extend my gratitude to Jason Langley, for his incredible patience and expertise in the many facets of this paper. I would also like to thank the entirety of the Center for Advanced Neuroimaging. Their technical and intellectual support was critical to the research, writing, and overall success of the project. I also wish to thank Dr. Begoña Echeverria and the entire University Honors team for their continuous support and for providing the framework and resources necessary to complete this capstone.

TABLE OF CONTENTS

1. Introduction

Magnetic resonance imaging (MRI) techniques to study the effects of normal aging or disease on brain tissue. Quantitative susceptibility mapping (QSM) is an MRI technique that measures magnetic susceptibility, the degree a material is magnetized in response to an applied magnetic field. Objects with a positive susceptibility are paramagnetic and objects with a negative susceptibility are diamagnetic. Quantitative susceptibility source separation allows for the separation of paramagnetic (i.e. positive susceptibility) and diamagnetic (i.e. negative susceptibility) components. Iron is paramagnetic and myelin is diamagnetic and the magnetic susceptibility of different tissues will vary based on the relative content of iron and myelin. Susceptibility source separation (χ-separation) is a QSM technique that separates the paramagnetic and diamagnetic susceptibility components within a single voxel. A high-resolution 3D gradient-echo sequence is needed to measure susceptibility in the cortex. With this sequence, researchers can visualize iron, blood, and calcification in the cerebral cortex. In addition, this technique has been used to quantify iron deposition and demyelination in the cortex of patients with pathology and in normal aging

In the brain, the main sources of diamagnetic susceptibility are myelin and calcium. Calcium tends to focus in focal areas, making it easily distinguishable from myelin. Thereby, myelin is the primary source of diamagnetic susceptibility map both in gray and white matter in healthy populations. Iron is the major source of paramagnetic susceptibility in the form of deoxyhemoglobin, ferritin, and hemosiderin. These sources appear more readily as the human brain ages in two ways: iron accumulation and demyelination. During normal aging, different regions of the brain will accrue iron at different rates. For example, the thalamus has an increase in susceptibility followed by a decrease around forty years of age. Cortical regions associated

with motor function show the highest increases in susceptibility (Burgetova et. al, 2021). Subcortical iron increases are often associated with neurodegeneration and cognitive decline in older adults. Studies also have shown that brain white matter susceptibility decreases (becomes more diamagnetic) from infant to teenage years, then increases linearly (becomes more paramagnetic) with aging, indicating a shift from myelination to demyelination (Liu et. al, 2016)

Excessive cortical iron is associated with accelerated cognitive decline, memory impairment, and development of neurogenerative diseases. For example, in Alzheimer's disease (AD) cortical iron has been shown to be elevated and has a strong association with the rate of cognitive decline (Ayton et. al, 2019). Increased iron levels in cortical regions have also been linked to worsened episodic memory, alongside overall lower executive function. Despite these clinical applications, how cortical susceptibility changes with normal aging has not been established. Establishing baseline susceptibility in normal aging is the first step in biomarker development. Here, age-related changes in grey matter occurring during normal aging is characterized. We will assess how diamagnetic and paramagnetic susceptibility components change with age in different cortical regions (frontal, temporal, occipital, and parietal lobes).

2. Methods

2.1.1 *Participants.* A total of 54 healthy human volunteers aged 60-87 years (interquartile range: 65-73, median: 68, mean: 69.3 ± 6.02 years; 24 males and 30 females) were recruited from the community surrounding the University of California, Riverside. They were evaluated to have normal general cognition (e.g., greater than 17 on the telephone Montreal Cognitive Assessment, MoCA; Pendlebury et al., 2013) and self-reported no major health conditions (e.g., stroke, dementia, diabetes) or conditions that would make MRI scanning unsafe or unpleasant (e.g., non-MR compliant implants, difficulty lying in the supine position, claustrophobia). All subjects

provided written informed consent. The study was reviewed and approved by the Institutional Review Board.

2.1.2 *Structural acquisition and processing.* Imaging data were acquired using a 3T Siemens Prisma (Prisma, Siemens Healthineers, Malvern, PA). Images from a T1-weighted magnetization prepared rapid gradient echo (MP-RAGE) sequence (echo time (TE)/repetition time (TR)/inversion time=3.02 / 2600 / 800 ms, flip angle=8°, voxel size=0.8 × 0.8 × 0.8 mm^3) were used for registration from subject space to common space. T1-weighted images were analyzed with FMRIB Software Library (FSL). A transformation was derived between individual subject space to MNI152 T1-weighted space using FMRIB's Linear Image Registration Tool (FLIRT) and FMRIB's Nonlinear Image Registration Tool (FNIRT) in the FSL software package. The transform to MNI152 space was derived using the follow steps: (1) The T_1-weighted image was skull stripped using the brain extraction tool (BET) in FSL, (2) brain extracted T_1-weighted images were aligned with the MNI brain extracted image using an affine transformation, and (3) a nonlinear transformation (FNIRT) was used to generate a transformation from individual T_1-weighted images to T_1-weighted MNI152 common space.

For each participant, grey matter, white matter, and cerebral spinal fluid (CSF) were segmented in the T1-weighted MP-RAGE image using FMRIB's Automated Segmentation Tool (FAST).

2.1.3 *Iron data acquisition.* A multi-echo gradient echo sequence is required to measure R_2*. Multi-echo data were collected with a 6-echo 3D gradient recalled echo sequence: TE1 /ΔTE /TR =4 / 6 / 40 ms, FOV=192 × 224 mm, matrix size=192 × 224 × 96, and slice thickness=1.7 mm.

2.1.4. *R_2* calculation*. R_2* was calculated from the magnitude data assuming a monoexponential decay. R_2 values were calculated voxelwise by fitting the signal from the 3D gradient echo with the following function:

$$S(T_E) = S_0 \exp(-T_E R_2)$$

where S_0 denotes a fitting constant, TE denotes the echo time. Characteristic R_2* images for a younger and an older participant are shown in Figure 1.

For each participant, a transform between the multi-echo acquisition and the T1-weighted MP-RAGE acquisition was derived using the first echo from the multi-echo acquisition using the following steps: (1) the first echo from the multi-echo acquisition was brain extracted using BET in FSL, (2) a linear transform to the T1-MP RAGE sequence was then derived using the brain extracted image from the first echo. This transform was then concatenated with the transform between the T1-weighted MP-RAGE sequence and MNI space and the concatenated transform was then inverted. This transform allows for standard space regions of interest to be transformed to the multi-echo gradient echo images with minimal interpolation.

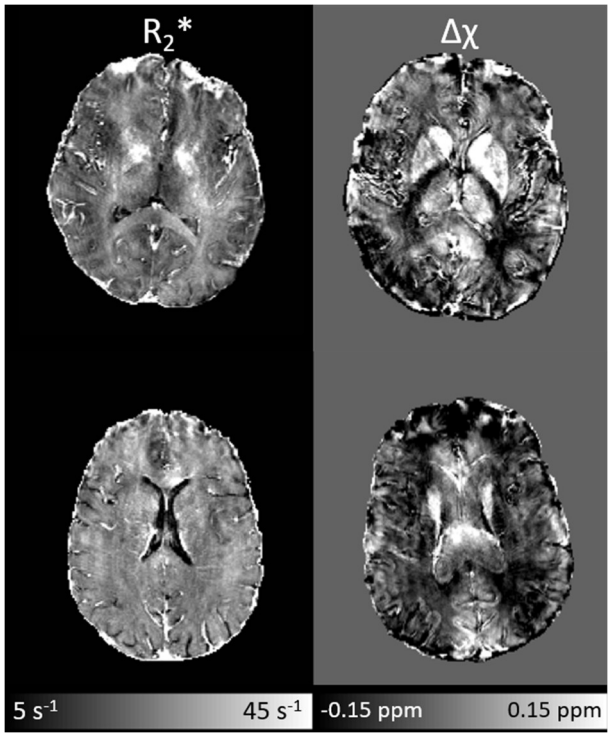

Figure 1. R_2* maps for a younger and older subject (left) and total susceptibility maps for a younger and older subject (denoted $\Delta\chi$; right).

2.1.5. *Susceptibility (χ) source separation*. To generate a χ-separation map, the χ-separation toolbox (https://github.com/SNU-LIST/chi-separation) was used. It is based on a biophysical model defining how paramagnetic susceptibility (χ_{para}) and diamagnetic susceptibility (χ_{dia}) affect the magnetic field perturbation (Δf) and the reversible transverse relaxation rate ($R'_2 = R_2^* - R_2$). The relationship is expressed as follows:

$$\Delta f = D_f^* (\chi_{para} + \chi_{dia}) \quad (1)$$

$$R_2' = D_{r,para} |\chi_{para}| + D_{r,dia} |\chi_{dia}|, \quad (2)$$

where D_f is the dipole kernel, and $D_{r,para}$ and $D_{r,dia}$ are the relaxometric constants relating R_2' to the paramagnetic and diamagnetic susceptibility, respectively. In this study, a neural network application of χ-separation, called χ-sepnet-R_2*, was used (https://github.com/SNU-LIST/chi-separation). χ-sepnet-R_2* was trained using multihead orientation data as targets to provide

streaking artifact-free χ_{para} and χ_{dia} maps. While traditional methods rely on R_2' as the input, this specific network was also trained to use R_2*, allowing for accurate mapping of χ_{para} and χ_{dia} without R_2.

A tissue field map (Δf) and an R_2* map were used as the inputs for χ-sepnet-R_2*. These inputs were obtained from the phase and magnitude components of a multiecho GRE sequence, respectively, via the following steps. First, the phase maps from the multiecho GRE data were unwrapped using the Laplacian-based unwrapping algorithm (*MRPhaseUnwrap*; STI Suite; https://people.eecs.berkeley.edu/~chunlei.liu/software.html). These maps were averaged using a signal-to-noise-ratio-weighted mean which made a combined phase map. A brain mask was then extracted and applied. This was then filtered to remove the background field by applying V-SHARP (STI Suite), generating a tissue field map (Δf). The R_2* map described in the previous section was applied alongside (Δf) in χ-sepnet-R_2*, producing χ_{para} and χ_{dia} maps which were combined to produce a total susceptibility map.

2.1.4 *Regions of interest*. A prior study parceling the cortex (Zhang et al., 2010) was used to define standard space regions of interest (ROIs) in the frontal lobe, temporal lobe, occipital lobe, and parietal lobe respectively. The ROIs were then transformed from MNI space to the iron-sensitive images in subject space using linear and nonlinear transforms in FSL as described in the earlier sections.

Each aligned ROI was thresholded at 60% and binarized. To ensure that the signal from white matter did not contaminate measures in each cortical region, the binarized ROI was multiplied by each individual's grey matter mask, derived from FAST. This process excluded voxels containing white matter and CSF from the susceptibility estimate and ensured that voxels containing grey matter were used in the susceptibility calculation. Diamagnetic and paramagnetic

susceptibilities were measured in each resultant ROI for each participant. The ROIs are visualized in Figure 2.

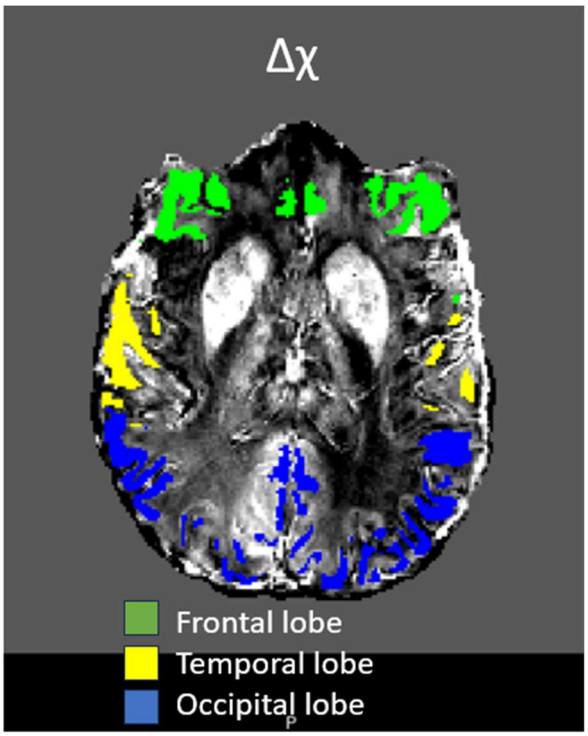

Figure 2. Cortical regions of interest of total susceptibility map (labeled Δχ).

2.1.6. *Statistics*. All statistical analyses were performed using MATLAB 2024b (The Mathworks Inc., Natick, MA, USA). Diamagnetic and paramagnetic susceptibilities in each ROI are reported as mean ± standard deviation. A p value less than 0.05 was considered significant for all group comparisons. Comparisons of diamagnetic and paramagnetic susceptibility were assessed separately using analysis of variance (ANOVA). Significant interactions were followed with post hoc between-group two-tailed t-tests for each region and susceptibility (diamagnetic, paramagnetic).

Relationships between age and diamagnetic susceptibility in each cortical region were assessed with separate Pearson correlations. Relationships between age and paramagnetic

susceptibility in each cortical region were assessed with separate Pearson correlations. A correlation was considered significant if it had a *P*-value less than 0.05.

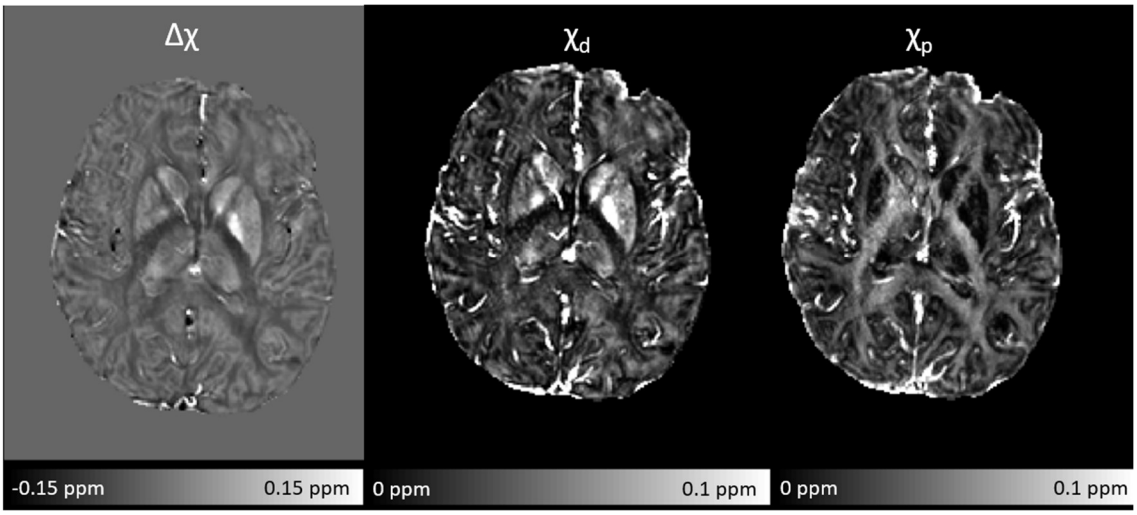

Figure 3. A comparison of total susceptibility (denoted Δχ; left), paramagnetic susceptibility (denoted χ_p; center), and diamagnetic susceptibility (denoted χ_d; right)

3. Results

3.1.1 *Age-diamagnetic susceptibility correlations*. A standard diamagnetic susceptibility image of a healthy brain is shown in the center of Figure 3, labeled as χ_d, which was derived using QSM. Statistically significant correlations were seen between age and diamagnetic susceptibility in the frontal lobe ($r = 0.412$, $p<0.01$). Similarly, statistically significant correlations were seen between age and diamagnetic susceptibility in the temporal lobe ($r = 0.286$, $p<0.01$). Statistically significant correlations were also seen between age and diamagnetic susceptibility in the occipital lobe ($r = 0.402$, $p<0.01$). Statistically significant correlations were seen between age and diamagnetic susceptibility in the parietal lobe ($r = 0.348$, $p<0.01$). These correlations are shown in Figure 4.

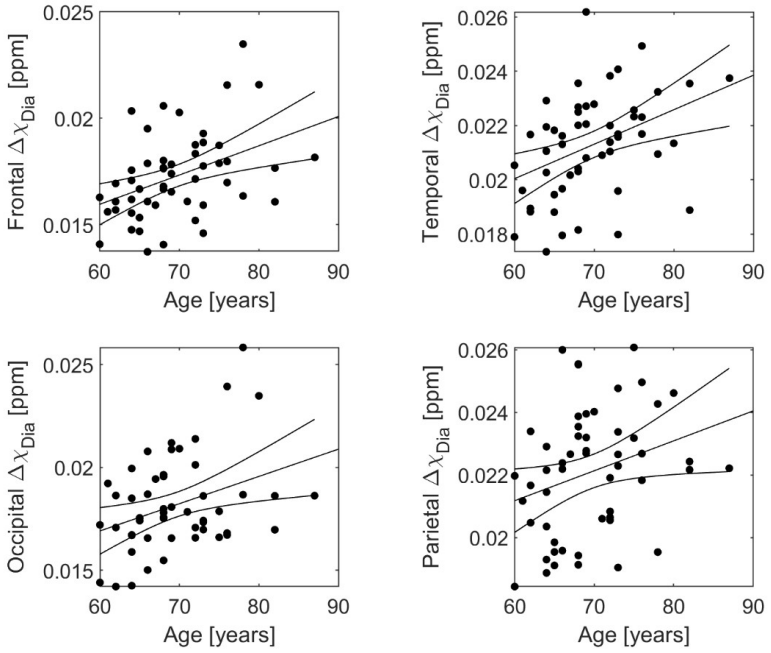

Figure 4. The relationship between diamagnetic susceptibility (denoted $\Delta\chi_{dia}$) and age across the four cortical ROIs for the temporal, frontal, parietal, and occipital lobes

3.1.2. *Age-paramagnetic susceptibility correlations*. A standard paramagnetic susceptibility image of a healthy brain is shown in the right column of Figure 3, labeled as χ_p, which was derived using QSM. No significant relationship was observed between age and the paramagnetic susceptibility component in the frontal lobe ($r = 0.083$, $p>0.05$). Similarly, no significant relationship was observed between age and the paramagnetic susceptibility component in the temporal lobe ($r = 0.088$, $p>0.05$). Positive association was seen between the occipital lobe paramagnetic susceptibility ($r = 0.323$, $p<0.05$) and age. A negative association was seen between the parietal lobe paramagnetic susceptibility and age ($r = -0.196$, $p<0.05$). These correlations are seen in Figure 5.

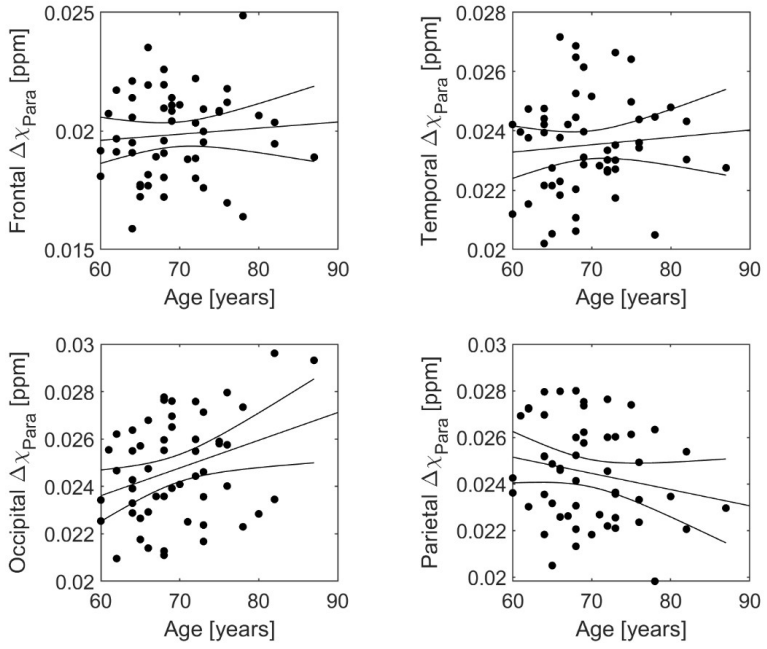

Figure 5. The relationship between paramagnetic susceptibility (denoted $\Delta\chi_{para}$) and age across the four cortical ROIs for the temporal, frontal, parietal, and occipital lobes

3.1.3. *Diamagnetic and paramagnetic susceptibilities across the ROIs*. An ANOVA revealed that each cortical region had differing diamagnetic susceptibilities ($F=68.3$, $p<0.01$). Step down t-tests revealed that higher diamagnetic susceptibility was seen in the temporal lobe (0.022 ppm ± 4.02E-06 ppm) relative to the susceptibility of the parietal lobe (0.018 ppm ± 5.25E-06 ppm). Step down t-tests revealed that higher diamagnetic susceptibility was seen in the frontal lobe (0.017 ppm ± 4.04E-06 ppm) relative to the susceptibility of the temporal lobe (0.022 ppm ± 4.02E-06 ppm). Step down t-tests revealed that higher diamagnetic susceptibility was seen in the frontal lobe (0.017 ppm ± 4.04E-06 ppm) relative to the susceptibility of the occipital lobe (0.021 ppm ± 5.25E-06 ppm). Step down t-tests revealed that lower diamagnetic susceptibility was seen in the temporal lobe (0.022 ppm ± 4.02E-06 ppm) relative to the susceptibility of the occipital lobe (0.021 ppm ± 3.62E-06 ppm). Step down t-tests revealed that higher diamagnetic susceptibility was seen in the occipital lobe (0.021 ppm ± 3.6E-06 ppm) relative to the

susceptibility of the parietal lobe (0.018 ppm ± 5.25E-06 ppm). These relationships are shown in Figure 6A.

An ANOVA revealed that each cortical region had differing paramagnetic susceptibilities ($F=69.3$, $p<0.01$). Step down t-tests revealed that higher paramagnetic susceptibility was seen in the temporal lobe (0.024 ppm ± 2.9E-06 ppm) relative to the susceptibility of the parietal lobe (0.024 ppm ± 4.56E-06 ppm). Step down t-tests revealed that higher paramagnetic susceptibility was seen in the frontal lobe (0.020 ppm ± 3.4E-06 ppm) relative to the susceptibility of the temporal lobe (0.024 ppm ± 2.9E-06 ppm). Step down t-tests revealed that higher paramagnetic susceptibility was seen in the frontal lobe (0.020 ppm ± 3.4E-06 ppm) relative to the susceptibility of the occipital lobe (0.025 ppm ± 4.7E-06 ppm). Step down t-tests revealed that higher paramagnetic susceptibility was seen in the frontal lobe (0.020 ppm ± 3.4E-06 ppm) relative to the susceptibility of the parietal lobe (0.024 ppm ± 4.56E-06 ppm). Step down t-tests revealed that higher paramagnetic susceptibility was seen in the temporal lobe (0.024 ppm ± 2.9E-06 ppm) relative to the susceptibility of the occipital lobe (0.025 ppm ± 4.7E-06 ppm). Step down t-tests revealed that lower paramagnetic susceptibility was seen in the parietal lobe (0.024 ppm ± 4.56E-06 ppm) relative to the susceptibility of the occipital lobe (0.025 ppm ± 4.7E-06 ppm). These relationships are shown in Figure 6B.

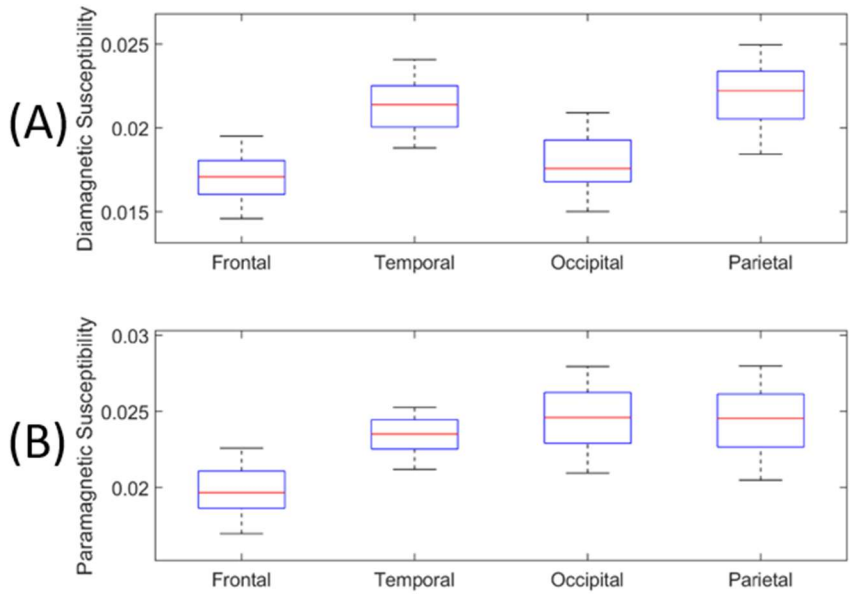

Figure 6. Comparison of diamagnetic susceptibility (χ_{dia}, shown in A) and paramagnetic susceptibility (χ_{para}, shown in B) across the four cortical regions.

4. Discussion

We examined the relationship between age and susceptibility (diamagnetic, paramagnetic) across four cortical regions (frontal, temporal, occipital, and parietal). We found that age was positively associated with diamagnetic susceptibility in the frontal, temporal, occipital, and parietal lobes. For paramagnetic susceptibility, we observed a positive association with age in the occipital lobe and a negative association with age in the parietal lobe. No statistically significant correlations were seen between paramagnetic susceptibility and age in the frontal or temporal lobes. ANOVA tests revealed that each cortical region had both differing diamagnetic and paramagnetic susceptibilities. Step down t-tests revealed that the parietal lobe had the highest diamagnetic susceptibility, followed by the temporal, occipital, and frontal lobes.

Prior work has found that grey matter volume decreases in the cortex of older adults.

This reduction in grey matter volume may increase the contribution of myelin to diamagnetic susceptibility and lead to higher diamagnetic susceptibility in the cortex (Hagemeier et. al, 2017). Alternatively, beta amyloid plaques (Aβ) tend to accrue in the cortex with age. These plaques, alongside tau neurofibrillary tangles, are hallmarks of Alzheimer's disease pathology (Gong et. al, 2019). Proteins tend to be diamagnetic due to their high concentrations of paired electrons. Aggregations of Aβ causes an increase in electron density, causing a large change in local susceptibility to generate contrast relative to surrounding normal tissues, showing a higher diamagnetic susceptibility (Babaei et. al, 2017).

Paramagnetic susceptibility can be assessed using susceptibility source separation and iron is the primary contributor to paramagnetic susceptibility in the brain (Lee et. al, 2024). We observed differing correlations between paramagnetic susceptibility in the parietal and occipital lobes. These differing correlations may be related to the rate of iron deposition in the cortex but additional work needs to be done to verify this result.

This technique may be applied to assess AD pathology. Currently, Aβ plaques and tau neurofibrillary tangles can only be assessed *in vivo* using positron emission tomography (PET) tracers. The radioligands for these tracers deposit ionizing radiation in AD patients and access is limited to major academic hospitals. As previously detailed, Aβ is diamagnetic and increases in the diamagnetic susceptibility component of AD patients may be related to Aβ deposition. The paramagnetic (positive susceptibility) component, is shown to be related to the tau (τ) tracer, which is commonly shown in early-stage AD (Langley et. al, 2025). Both τ and amyloid have negative susceptibility (i.e. diamagnetic), so we would also expect there to be a positive correlation solely from τ buildup (Gong et. al, 2019).

The accuracy of susceptibility measurement in the temporal lobe and frontal lobe is reduced due to magnetic field homogeneity in these regions. The phase is affected by magnetic field inhomogeneities and it may be not be possible to accurately remove them during the susceptibility calculation. This result in uncertainty in the susceptibility in these regions and may explain the lack of correlation between the paramagnetic susceptibility with age in the frontal and temporal lobes.

5. Conclusion

We were able to assess how diamagnetic and paramagnetic susceptibility components change with age in the frontal, temporal, occipital, and parietal lobes. Through the usage of QSM, we were also able to establish a healthy baseline for what the brain should look like in these regions. This will allow future studies to be able to make comparisons between normal aging brains and brains suffering from neurodegenerative diseases.

References

1. Ayton, S., Wang, Y., Diouf, I., Schneider, J. A., Brockman, J., Morris, M. C., & Bush, A. I. (2019). Brain iron is associated with accelerated cognitive decline in people with Alzheimer pathology. *Molecular Psychiatry*, *25*(11), 2932–2941. https://doi.org/10.1038/s41380-019-0375-7
2. Babaei, M., Jones, I. C., Dayal, K., & Mauter, M. S. (2017). Computing the Diamagnetic Susceptibility and Diamagnetic Anisotropy of Membrane Proteins from Structural Subunits. *Journal of Chemical Theory and Computation*, *13*(6), 2945–2953. https://doi.org/10.1021/acs.jctc.6b01251
3. Bulk, M., Abdelmoula, W. M., Nabuurs, R. J., Van Der Graaf, L. M., Mulders, C. W., Mulder, A. A., Jost, C. R., Koster, A. J., Van Buchem, M. A., Natté, R., Dijkstra, J., & Van Der Weerd, L. (2017). Postmortem MRI and histology demonstrate differential iron accumulation and cortical myelin organization in early- and late-onset Alzheimer's disease. *Neurobiology of Aging*, *62*, 231–242. https://doi.org/10.1016/j.neurobiolaging.2017.10.017
4. Burgetova, R., Dusek, P., Burgetova, A., Pudlac, A., Vaneckova, M., Horakova, D., Krasensky, J., Varga, Z., & Lambert, L. (2021). Age-related magnetic susceptibility changes in deep grey matter and cerebral cortex of normal young and middle-aged adults depicted by whole brain analysis. *Quantitative Imaging in Medicine and Surgery*, *11*(9), 3906–3919. https://doi.org/10.21037/qims-21-87
5. Cogswell, P. M., Wiste, H. J., Senjem, M. L., Gunter, J. L., Weigand, S. D., Schwarz, C. G., Arani, A., Therneau, T. M., Lowe, V. J., Knopman, D. S., Botha, H., Graff-Radford, J., Jones, D. T., Kantarci, K., Vemuri, P., Boeve, B. F., Mielke, M. M., Petersen, R. C., &

Jack, C. R. (2020). Associations of quantitative susceptibility mapping with Alzheimer's disease clinical and imaging markers. *NeuroImage*, *224*, 117433. https://doi.org/10.1016/j.neuroimage.2020.117433

6. Connor, J. R., Snyder, B. S., Beard, J. L., Fine, R. E., & Mufson, E. J. (1992). Regional distribution of iron and iron-regulatory proteins in the brain in aging and Alzheimer's disease. *Journal of Neuroscience Research*, *31*(2), 327–335. https://doi.org/10.1002/jnr.490310214
7. Deh, K., Ponath, G. D., Molvi, Z., Parel, G. T., Gillen, K. M., Zhang, S., Nguyen, T. D., Spincemaille, P., Ma, Y., Gupta, A., Gauthier, S. A., Pitt, D., & Wang, Y. (2018). Magnetic susceptibility increases as diamagnetic molecules breakdown: Myelin digestion during multiple sclerosis lesion formation contributes to increase on QSM. *Journal of Magnetic Resonance Imaging*, *48*(5), 1281–1287. https://doi.org/10.1002/jmri.25997
8. Faul, F., Erdfelder, E., Buchner, A., & Lang, A.-G. (2009). Statistical power analyses using G*Power 3.1: Tests for correlation and regression analyses. *Behavior Research Methods*, *41*, 1149-1160.
9. Gong, N., Dibb, R., Bulk, M., Van Der Weerd, L., & Liu, C. (2019). Imaging beta amyloid aggregation and iron accumulation in Alzheimer's disease using quantitative susceptibility mapping MRI. *NeuroImage*, *191*, 176–185. https://doi.org/10.1016/j.neuroimage.2019.02.019
10. Hagemeier, J., Zivadinov, R., Dwyer, M. G., Polak, P., Bergsland, N., Weinstock-Guttman, B., Zalis, J., Deistung, A., Reichenbach, J. R., & Schweser, F. (2017). Changes of deep gray matter magnetic susceptibility over 2 years in multiple sclerosis and healthy

control brain. NeuroImage Clinical, 18, 1007–1016. https://doi.org/10.1016/j.nicl.2017.04.008

11. Hardy, J. A., & Higgins, G. A. (1992). Alzheimer's Disease: The Amyloid Cascade hypothesis. *Science*, *256*(5054), 184–185. https://doi.org/10.1126/science.1566067
12. Kopp W. Aging and "Age-Related" Diseases - What Is the Relation?. *Aging Dis*. 2024;16(3):1316-1346. Published 2024 Jun 28. doi:10.14336/AD.2024.0570
13. Langley, J., Bennett, I. J., Hu, X. P., & Initiative, F. T. a. D. N. (2024). Examining iron-related off-target binding effects of 18 F-AV1451 PET in the cortex of Aβ+ individuals. *European Journal of Neuroscience*, *60*(1), 3614–3628. https://doi.org/10.1111/ejn.16362
14. Langley, J., Solis, K., Masjedizadeh, V., Shao, M., Bennett, I., & Hu, X. P. (2025, May 15). *Associations between iron and mean kurtosis in iron-rich grey matter nuclei in aging*. https://pmc.ncbi.nlm.nih.gov/articles/PMC12133083/
15. Lebel, C., & Deoni, S. (2018). The development of brain white matter microstructure. NeuroImage, 182, 207–218. https://doi.org/10.1016/j.neuroimage.2017.12.097
16. Lee, J., Ji, S., & Oh, S. (2024). So you want to image myelin using MRI: magnetic susceptibility source separation for myelin imaging. *Magnetic Resonance in Medical Sciences*, *23*(3), 291–306. https://doi.org/10.2463/mrms.rev.2024-0001
17. Liu, H., Yang, Y., Xia, Y., Zhu, W., Leak, R. K., Wei, Z., Wang, J., & Hu, X. (2016). Aging of cerebral white matter. *Ageing Research Reviews*, *34*, 64–76. https://doi.org/10.1016/j.arr.2016.11.006
18. Meadowcroft, M. D., Connor, J. R., Smith, M. B., & Yang, Q. X. (2009). MRI and histological analysis of beta-amyloid plaques in both human Alzheimer's disease and

APP/PS1 transgenic mice. *Journal of Magnetic Resonance Imaging*, *29*(5), 997–1007. https://doi.org/10.1002/jmri.21731

19. Min, K., Sohn, B., Kim, W. J., Park, C. J., Song, S., Shin, D. H., Chang, K. W., Shin, N., Kim, M., Shin, H., Lee, P. H., & Lee, J. (2024). A human brain atlas of χ-separation for normative iron and myelin distributions. *NMR in Biomedicine*, *37*(12), e5226. https://doi.org/10.1002/nbm.5226
20. Sisodia, S. S., & Price, D. L. (1995). Role of the β-amyloid protein in Alzheimer's disease. *The FASEB Journal*, *9*(5), 366–370. https://doi.org/10.1096/fasebj.9.5.7896005
21. Spotorno, N., Acosta-Cabronero, J., Stomrud, E., Lampinen, B., Strandberg, O. T., Van Westen, D., & Hansson, O. (2020). Relationship between cortical iron and tau aggregation in Alzheimer's disease. *Brain*, *143*(5), 1341–1349. https://doi.org/10.1093/brain/awaa089
22. Van Bergen, J. M. G., Li, X., Hua, J., Schreiner, S. J., Steininger, S. C., Quevenco, F. C., Wyss, M., Gietl, A. F., Treyer, V., Leh, S. E., Buck, F., Nitsch, R. M., Pruessmann, K. P., Van Zijl, P. C. M., Hock, C., & Unschuld, P. G. (2016). Colocalization of cerebral iron with Amyloid beta in Mild Cognitive Impairment. *Scientific Reports*, *6*(1), 35514. https://doi.org/10.1038/srep35514